Biomagnetic functional localization of a peripheral nerve in man

Lutz Trahms,* Sergio N. Erné,* Zvonko Trontelj,* Gabriel Curio,‡ and Peter Aust‡
*Physikalisch-Technische Bundesanstalt, Institut Berlin, D-1000 Berlin 10; and ‡Department of Neurology, Klinikum Steglitz, Freie Universität Berlin, D-1000 Berlin 45, Federal Republic of Germany

ABSTRACT The first detection of the magnetic field of a stimulated peripheral nerve in man is presented. The measurement was performed noninvasively and in vivo on a healthy subject. The spatio-temporal field distribution is utilized to calculate the location of bioelectric activity on the basis of the equivalent current dipole model. The localization of the active nerve tissue is confirmed by a computer tomography image of the upper arm cross-section. Furthermore, a calculation of the total current distribution in the nerve explains the observed morphology of the signal.

1. INTRODUCTION

The development of noninvasive techniques to determine the site of physiologic processes in the human body is a challenging task in medical physics. In preoperative diagnostics, the localization of pathologic functions, such as the electric activity of epileptogenic brain tissue, is of particular relevance. This cellular malfunction generates a weak magnetic field that can be measured noninvasively in the vicinity of the source. The distribution of this magnetic field can be utilized to determine the location of the source. However, this localization refers to an equivalent current source and ignores the spatial extension of the real current distribution. In addition, the effect of inhomogeneity in the tissue on the measured magnetic field cannot be calculated for a real situation. Therefore, some uncertainty remains as to what extent a source localization based on a magnetic field distribution represents the location of the real source.

A pragmatic way to explore this is the comparison of biomagnetic localizations with independent experimental evidence. Some successful validation studies have been reported in the recent years. Biomagnetic sources in the brain of epileptic patients, localized with one- or multichannel gradiometers, have been shown by Ricci and co-workers (1) to coincide with the position of pathologic tissue, as identified using imaging techniques. Sutherling and co-workers recently correlated the results of invasive examinations, employing intracranial depth electrodes, with magnetically obtained localizations of epileptogenic foci (2).

Studies such as these are confined to patients with special pathological disorders which require invasive diagnostic or surgical intervention. In addition, implications based on these validations are limited by inherent methodical constraints: (*a*) When comparing the biomagnetically determined location of a current source with an anatomic lesion detected by x-ray computer tomography (CT) or magnetic resonance images (MRI), one has to realize that this lesion solely indicates a region of irregular tissue property, but not necessarily the relevant region of functional pathology. (*b*) As pointed out by Sutherling and co-workers (3), intracranial depth electrodes cannot sample from all parts of the brain. In particular, currents deep in the brain that mutually cancel in a closed field will not be detected unless the electrode terminals are brought right into the source.

In this study, we report our experience with a new procedure to validate neuromagnetic localizations that is applicable to normal subjects. We have chosen a stimulated peripheral nerve to determine the position of the active tissue on the basis of the magnetic field distribution. This approach has a number of advantages: (*a*) The techniques to stimulate peripheral nerves are well established in electrophysiology and easy to perform. (*b*) The tissue of a peripheral nerve represents a well-defined small volume, which is practically a one-dimensional conductor (its diameter is <4 mm). (*c*) It is possible to localize the position of the nerve tissue with high spatial resolution by independent methods, such as CT or MRI. (*d*) The fundamental electric characteristics of this current source are known.

On the other hand, there is the difficulty that the magnetic field of a stimulated nerve is weak. Presumably this is why only a few recordings of magnetic compound action fields (MCAFs) have been published so far. As early as 1980, Wikswo and co-workers detected the MCAF of the frog sciatic nerve threaded through a toroid recording coil (4). Many further studies of this group on

Dr. Trontelj's permanent address is University E. Kardelj of Ljubljana, Physics Department, YU-61000 Ljubljana, Yugoslavia.

the magnetic fields of peripheral nerves followed, among these the first in vivo detection of the MCAF of a primate, measured intraoperatively with a similar setup (5). Attempts to noninvasively detect the MCAF of human subjects have hitherto failed (6). Moreover, recordings of magnetic field distributions of peripheral nerves have not been reported to date. However, such magnetic maps are the prerequisite for the application of a localization procedure.

In a recent congress note, we reported the first detection of the magnetic field of a human peripheral nerve in vivo (7). Here we present subsequent work based on these preliminary studies. We have recorded a MCAF distribution to calculate the position of the equivalent source. This result was compared with the position of the nerve tissue determined by x-ray CT images. Finally, we have applied the established model of impulse propagation in nerves to the generation of compound current distributions. This calculation of the entire current provides some insight into the applicability of the equivalent current dipole model used in the localization procedure.

2. EXPERIMENTAL PROCEDURES

The experiments presented here were performed with one of the authors (P. Aust) as volunteer. The technical details of the procedure are described in the following paragraphs.

a. Paradigma

The median nerve of the right arm was stimulated by a rectangular current pulse applied by a standard bipolar stimulator at the wrist with the cathode at the proximal position. The position of the two electrodes was adjusted by maximizing the motoric effect of a constant current pulse. For the biomagnetic measurements the amplitude of the stimulation was kept below the motor threshold, at values below 15 mA with a voltage limit of 100 V. The duration of a single pulse was 100 μs, the repetition rate 10 Hz.

b. Experimental configuration

The geometry of the setup is sketched in Fig. 1 *a*. Here the axes x and y indicate only the orientation of the measuring plane, not the position of the origin of the coordinate frame. To define the geometrical parameters precisely, it is helpful to use the simplified picture of Fig. 1 *b*. The x-axis is along the long axis of the nerve and points in the direction of the stimulus propagation; the z-axis is in the direction of the radius vector pointing from the central axis of the arm to the position of the nerve. The z-direction is parallel to the axis of the magnetometer pickup coil; x and y define the plane where the measuring positions of the center of the coil are located. The origin of the reference frame is chosen such that x and y are zero at the stimulator cathode, and z is zero in the measuring plane.

The real situation differs significantly from this idealized picture, of course. The transfer of these definitions to the experimental setup can be based on estimations only. However, this does not restrict the precision of the procedure, as long as the geometry is reproducible. The orientation of the x-y plane is given by estimating the orthogonal connection of

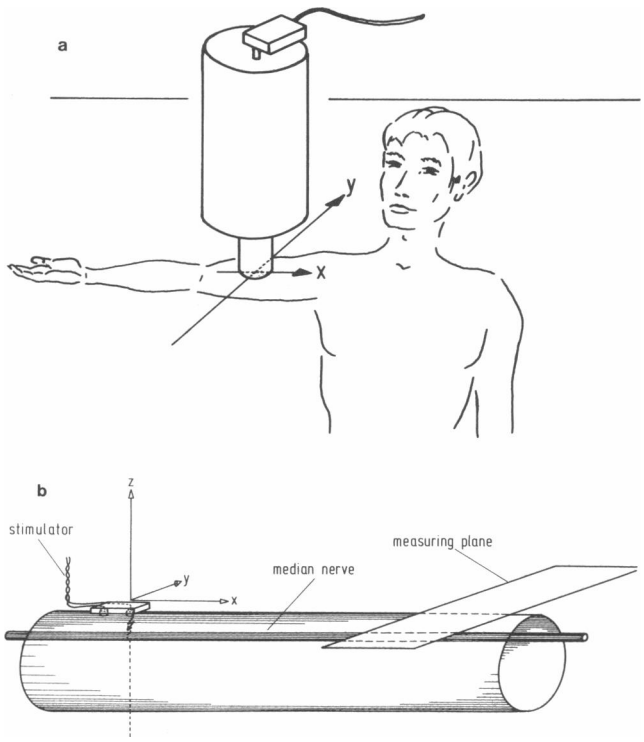

FIGURE 1 Geometry of the experiment. (*a*) Sketch of the experimental setup. The detection coil is at the bottom of the dewar tail. x and y indicate only the direction of the reference frame, with the axis of the pickup coil perpendicular to the measuring plane, xy. (*b*) Simplified sketch to define both origin and orientation of the reference frame. Details are given in the text of section 2 *b*.

the central axis of the upper arm and the nerve. To realize this geometry, the arm was fixed in a cast, and a plastic ruler was attached to it in the defined orientation. This arrangement could be reproduced for the CT recording with a maximal error of $\Delta y = \pm 1$ mm with regard to the position of the origin, and $\Delta\theta = \pm 5°$ with regard to the orientation of the z-axis, θ. The x-y plane with $z = 0$, where the center of the recording coil was positioned, was defined at a distance of 24 mm above the surface of the skin.

c. Detection system

The measurements were performed in the Berlin Magnetically Shielded Room (8). Electric and magnetic signals were recorded simultaneously, using two channels of a 15-channel biosignal acquisition system (9). The electric measurements were made with conventional cup electrodes filled with contact jelly. The potential at the ipsilateral acromion was taken as reference, the ground electrode was attached to the forearm, between stimulation and recording electrodes. The impedances of the electrodes were below 1 kΩ.

Magnetic fields were measured with a single channel magnetometer. This device consisted of a five-turn pickup coil with 40 mm diameter and an interwinding distance of 1.5 mm. The magnetic flux was transformer-coupled to a radio-frequency Superconducting Quantum Interference Device (the two-hole Zimmerman type of a RF-SQUID [10]). The noise level of the entire detection system in the empty shielding chamber was below 8 ft/$\sqrt{\text{Hz}}$.

The signals were filtered with a first order RC-high pass at 5 Hz and an eighth order Bessel low pass at 1,500 Hz. In addition, a special filter against 50 Hz and harmonics of the power line was installed for the magnetic channel (11). Using the stimulus pulse as trigger, epochs of 20 ms duration were recorded and digitally stored with 10 kHz sampling rate. At one measuring position, typically 4,000 epochs were acquired for the subsequent off-line averaging procedure.

d. Validation

The position of the nerve was validated with a two-dimensional x-ray CT image of the upper arm cross-section. These pictures were taken with the CT equipment of the radiology department at the Klinikum Steglitz of the Freie Universität Berlin. To obtain unequivocal confirmation of the location of the nerve tissue, a contrast enhanced CT scan sequence was performed at well-defined time intervals after a bolus injection of 20 ml contrast agent into the contralateral hand vein.

3. THEORY

The magnetic field **B** generated by a current distribution $\mathbf{j}(\mathbf{r}')$ inside a volume V can be described in terms of a current multipole expansion (12)

$$\mathbf{B}(\mathbf{r}) = (\mu_0/4\pi)\,\mathrm{curl}\,(r^{-1}\mathbf{J} + r^{-3}\mathbf{r}\underline{\underline{Q}} + \cdots), \qquad (1)$$

where μ_0 is the permeability constant, and $\mathbf{r} = (r_x, r_y, r_z)$ refers to the position of the multipole as origin. The structure of the current source is given by the multipole terms, $\mathbf{J}$,$\underline{\underline{Q}}$, etc. The first element of this expansion, the current dipole, is given by

$$\mathbf{J} = \int_V \mathbf{j}(\mathbf{r}')\,d^3r'. \qquad (2)$$

As pointed out in the introduction, the study of the peripheral nerve was motivated by the expectation that this simple source will generate a simple field. As a first approach it is therefore adequate to employ the most simple model of a bioelectric source, the equivalent current dipole. The z-component of the magnetic field generated by this source is given by (13)

$$B_z(\mathbf{r}) = (\mu_0/4\pi)\,r^{-3}\,(J_x r_y - J_y r_x). \qquad (3)$$

The recorded data represent the magnetic field sensed by the five turns of the detection coil. Location and radius of the loops are given by the position of the center of the coil and the arrangement of the windings with respect to this point (see section 2. *c*). The integration over the loop is carried out in a straightforward way (12, 14), using standard tables when calculating elliptic integrals of the first and second kind.

The position of the model source, the equivalent current dipole, is determined by a standard best fit algorithm which varies the five parameters: coordinates of the source in the three-dimensional half-space below the measuring plane, and the components of the dipole in the x-y plane, J_x and J_y. Following the procedure described above, the averaged magnetic field generated by the equivalent source is calculated. The ouput of the computer program is the set of parameters that yields the smallest deviation of calculated and measured field distribution.

4. RESULTS AND DISCUSSION

a. Pilot experiments

For the convenience of the reader we will first briefly summarize the results of our study on the identification of the magnetic activity of a peripheral nerve. This has already been published in a congress note (7). In Fig. 2 *a* the temporal development of the magnetic field of the stimulated median nerve is plotted for three sensor positions along the x-axis. With increasing x, the magnetic signals exhibit an increasing delay with respect to the instant of stimulation, $t = 0$. This reflects the propagation of the action potential toward the shoulder with a velocity between 50 and 60 m/s.

Fig. 2 *b* shows the magnetic recordings at two y-coordinates of opposite sign, i.e., ventral and dorsal of the median nerve. The polarity reversal reflects the bipolar pattern of the MCAF, consistent with a model of the equivalent current dipole pointing into the x-direction.

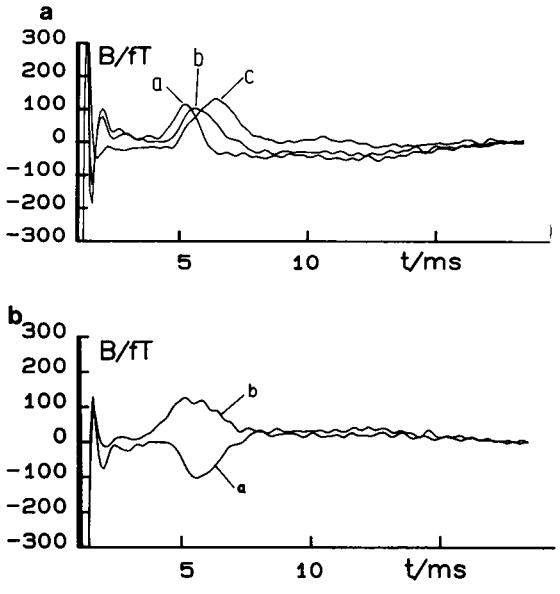

FIGURE 2 Magnetic field after stimulation at $t = 0$, and $x = 0$. (*a*) Propagation. Three traces were recorded at $y = 30$ mm, and (*i*) $x = 285$ mm, (*ii*) $x = 335$ mm, (*iii*) $x = 385$ mm. (*b*) Polarity reversal. Two traces were recorded at $x = 335$ mm and (*i*) $y = -30$ mm, (*ii*) $y = 30$ mm. These data were published previously (7).

These observations motivated the subsequent experiment in which a systematic spatial scan was performed to provide the data for a localization of the source.

b. Two-dimensional localization

A scan along the x-direction would mainly serve to determine the x-coordinate of the source. For our purpose this information is of little value. The real source is a distribution of currents in the nerve tissue extending several centimeters along the x-axis. A localization of the equivalent current dipole in this dimension can hardly be confirmed by other validation methods. Therefore, only the y-coordinate was varied for a fixed x-value. As a consequence of this restriction, the localization is confined to the position of the source in the y-z plane for a given x. We refer to this procedure as two-dimensional localization.

The stacked plot of Fig. 3 *a* shows the result of a ventro-dorsal scan. It was performed at the middle of the upper arm at a distance of $x = 335$ mm from the stimulator cathode at the wrist. The data of the individual positions are averages of 4,000 recordings. The first two milliseconds are disturbed by the artifact of the stimulator pulse at $t = 0$. The maximum magnetic field of the nerve is seen between 5 and 7 ms, the time interval when the equivalent current dipole passes the scanning line. The extremum at $t_m = 6.4$ ms corresponds to a mean propagation velocity $v_x = 52.3$ m/s. Note that this value represents only the x-component of the propagation velocity, v_y and v_z are not taken into account. If we assume a constant value of v, this implies that deviations of the course of the nerve from the x-direction lead to changes of the instantaneous value of v_x. In accordance to the simplified geometry of Fig. 1 *b*, such variations of v_x are ignored, and a constant propagation velocity of the equivalent current dipole, $v = (v_x, 0, 0)$, is assumed.

One way to process the data is to utilize the magnetic field values for one instant. This data set can serve as the basis of a linear field distribution, which can be fitted according to Eq. 3. However, this approach has some disadvantages: (*a*) The amount of data utilized in the localization procedure is small compared with the amount of available data. (*b*) There is no easy way to determine the instant when the equivalent current dipole passes the scanning line. This is necessary to determine the value for r_x and r which appear in Eq. 3. (*c*) A deviation of the dipole orientation from the x-direction in the x-y plane, that is, for a finite J_y, is not considered in this model.

To avoid these difficulties we have used a different approach. We describe the signal propagation in the nerve by an equivalent current dipole traveling along the x-axis with a constant velocity. With the transformation $v_x t = x'$, the second dimension of a spatial scan is generated and

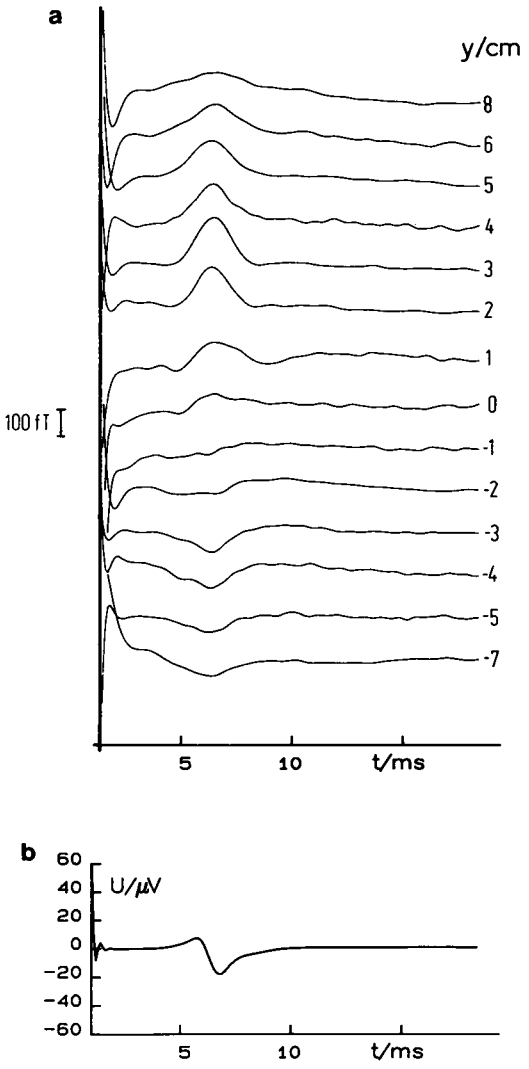

FIGURE 3 (*a*) Linear scan of the magnetic recording along the y-axis. (*b*) Electric potential recorded simultaneously at $y = 0$ mm and $x = 335$ mm.

the recorded data are considered the elements of a two-dimensional field distribution in the x'-y plane.

With this view, the amount of data available for a localization program has increased considerably. The time interval during which the equivalent current dipole generates a detectable magnetic signal has a length of 2 ms centered around the instant of maximum magnetic field intensity. With 10 kHz sampling frequency the 14 y-positions yield a total data set of 280 points. The 1.5 kHz low pass makes this set redundant by a factor of three or four, so it is appropriate to reduce the data set by extracting five equidistant points along the x'-direction. The magnetic field values at these 70 positions are taken as the basis of a two-dimensional field map. To visualize

this set of input data, Fig. 4 shows the magnetic field distribution in a sketch of isofield lines, which are generated by an interpolation algorithm. The pattern clearly shows the dipolar structure of the source.

The best fit algorithm applied to the 70 element data set optimizes five parameters that characterize the equivalent source: two components of the equivalent current dipole, J'_y and J_x, and the position of the source in the reference frame, given by the three components x', y, and z. This source generates the field most similar to the measured data. The parameters of the equivalent current dipole obtained in this way are

$$J'_y = 0.4 \text{ nA} \cdot \text{m}$$
$$J_x = 5.9 \text{ nA} \cdot \text{m}$$
$$x' = 330 \text{ mm}$$
$$y = -4 \text{ mm}$$
$$z = -40 \text{ mm}.$$

The field of this equivalent source has a standard deviation of 8% with respect to the measured data.

J'_y corresponds to the propagation of the equivalent current dipole in the y-direction, and is derived from the mean value of v_y over the considered time interval of 2 ms. It must be pointed out that J'_y is not identical with the real y-component of the equivalent current dipole, J_y, that would have been obtained had the data set been the result of an instantaneous two-dimensional scan in the x-y plane. However, there is a strong correlation between J_y and J'_y, because in peripheral nerves the directions of impulse propagation and the intraaxonal ionic currents are equal. Because $J'_y/J_x < 0.1$, we can assume that J_y is also small and can be neglected against J_x. As the measuring plane was chosen parallel to the idealized nerve, also J_z will be negligible, and we may consider J_x a good estimate of the equivalent current dipole intensity $J = (J_x^2 + J_y^2 + J_z^2)^{1/2}$. However, a quantitative discussion of this value is difficult due to the limited knowledge about the real current source, especially considering the result of the theoretical model studies presented in section 4 *c*. The result for x' confirms the input parameter $v_x = 52.3$ m/s, because the relation $v_x t = x'$ is satisfied with a slight deviation of 1.5%. A significant improvement of the procedure by a recursive correction of the input parameter, v_x, cannot be expected.

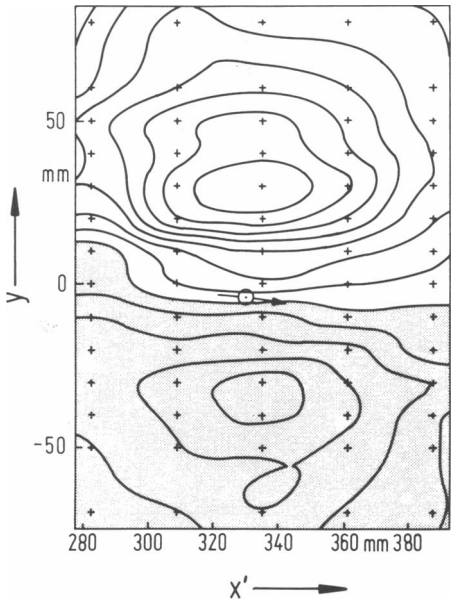

FIGURE 4 Isofield pattern in the x'-y plane with 20 fT steps between two isofield lines. Crosses indicate the positions of the 70 input data points. Shaded area represents regions of negative B_z. The orientation of the equivalent current dipole is indicated by the arrow in the center of the map, its position in the x'-y plane is given by the dot at the midpoint of the arrow.

The most important results concern the source parameters y and z, of course, because these coordinates represent the biomagnetic localization in the cross-section of the arm. An independent indication of the source position is given in Fig. 5, which shows the corresponding CT image of the arm taken in the localization plane, for $x = 335$ mm. The tissue of the median nerve is identified as the kidney-shaped structure deep in the sulcus bicipitalis medialis adjacent to the arteria and vena brachialis, which are enhanced by a contrast agent. The relation to the y and z component of the biomagnetic localization is provided by the position of the plastic ruler reconstructed in the CT image. The agreement between the functional biomagnetic localization and the structural x-ray image is quite satisfactory: the location is at the edge of the nerve cross-section. The deviation of 2 mm from the center of the nerve is within the reproducibility of the geometric arrangement.

This result was obtained without considering volume currents outside the nerve tissue. In a homogeneous half space the contribution of these secondary currents to the vertical component of the biomagnetic field integrates to zero (15). The experimental situation, however, was different. The upper arm has a cylindrical shape rather than the Cartesian geometry of the half space. Secondary currents in such volume conductors can be simulated by introducing virtual sources perpendicular to the surface (16). These sources can be neglected for the magnetic field component normal to the surface of the volume. In our experiment, however, the detection coil axis was kept parallel to the Cartesian z-axis. Thus, one can expect pronounced contributions of volume currents to the measured field, B_z. These contributions might be influenced by the asymmetric arrangement of the tissue surrounding the nerve, as is evident from Fig. 5. The elements of the

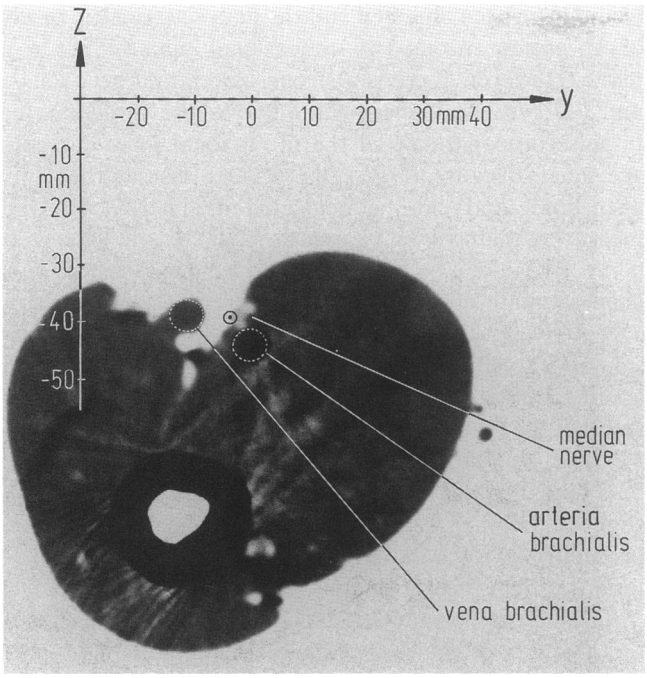

FIGURE 5 CT cross-section of the volunteer's right upper arm at x = 335 mm as seen in the distal direction. To preserve the quality of the image when processing the photograph, we reversed the contrast. Arteria and vena brachialis appear dark due to the contrast agent. The grey, kidney-shaped structure adjacent to the arteria brachialis represents the tissue of the median nerve. The reference frame is included in this picture to illustrate the result of the biomagnetic localization. The position of the equivalent current dipole determined in this study is indicated by the encircled dot at the edge of the median nerve.

conductivity tensor of the tissues involved, such as bone, muscle, fat, etc., differ considerably (17–19). Therefore, the impact of volume currents can be estimated by the asymmetry of the observed MCAF with respect to the y = 0 plane. In fact, the asymmetry of the amplitude of B_z, as evident from Fig. 3 and 4, is striking: for $y < 0$ the field is about two times weaker than for $y > 0$.

These considerations yield the result that, for the experimental circumstances described here, the effect of volume currents on the biomagnetic field is by no means negligible. It is likely that in some regions 50% or even more of the observed magnetic field is generated by volume currents. On the other hand, the location of the source was calculated with satisfactory precision. This seems to indicate that, for the conditions of this experiment, the determination of the source position is quite insensitive to such distortions. This may not apply for the other open parameters of the best fit, the equivalent current dipole orientation and intensity. Fortunately, these latter results are of minor relevance for clinical applications.

c. Compound current distribution

These calculations were based on the equivalent current dipole model using only the first element of the current multipole expansion. The real current in a stimulated peripheral nerve is a superposition of currents in some 5,000 axons. In each of these fibers, the axial current, I_x, varies in time as sketched in Fig. 6 *a*. This function is the derivative of the action potential, calculated on the basis of the theory of Hodgin and Huxley (20, 21). The absolute value of the amplitude in Fig. 6 *a* is a rough estimate, assuming a single axon of 10 μm diameter, and 0.5 $m^{-1}\Omega^{-1}$ longitudinal conductivity (22). The positive part of I_x describes the axial depolarization current, the negative part represents the axial repolarization current. These two parts are not symmetric with respect to each other due to the difference of the radial transmembrane current densities of sodium inflow during depolarization and potassium outflow during repolarization.

Replacing the argument of this function, $I_x(t)$, by $u = t - x/v_x$ yields a description of the propagation of this current pattern in time and space. The compound current

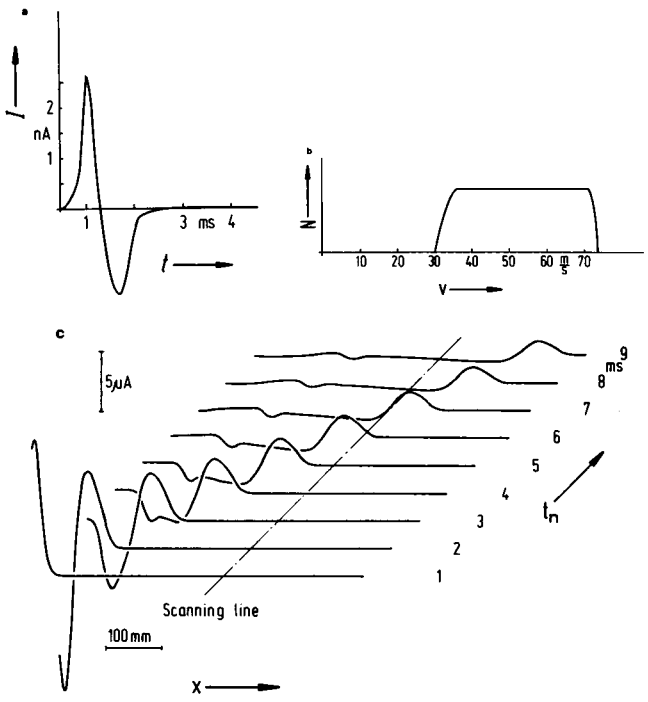

FIGURE 6 Illustration of the model calculation of the compound action current. The first two figures characterize the input functions. (*a*) The assumed temporal development of the action current in a single fiber for some fixed position, x. (*b*) Sketch of the assumed velocity distribution. (*c*) Stacked plot of the calculated compound action current along the x-axis at different instants, t_n. Broken line indicates the position of the detection loop.

of the nerve bundle is the superposition of the single fiber currents

$$I_{comp}(x, t) = \sum_i I_x (t - x/v_x^i), \quad (4)$$

where the summation is carried out over the currents in the single fibers, characterized by their individual velocity, v_x^i. The distribution of propagation velocities in peripheral nerves varies significantly, among different individuals as well as upon changes of the stimulus intensity (22–24). There is no justification to consider any particular distribution reported in the literature to be valid for the subject investigated here. However, they have in common a finite amount of fibres with velocities between 30 and 70 m/s. Usually, the distribution of fibers increases slightly toward higher velocities and decreases rapidly at 70 m/s. To keep the discussion most general we did not include these details in the model calculation of $I_{comp}(x, t)$ but assumed a most simple situation sketched in Fig. 6 *b*. This velocity distribution is constant over an interval between 35 and 70 m/s, decreasing rapidly at the edges.

Fig. 6 *c* shows $I_{comp}(x)$ for a number of instants, t_n, calculated for 5,000 axons with this velocity distribution. The uncertainty of the amplitude is more than one order of magnitude so that, again, a quantitative discussion in terms of the current intensity is without relevance. From the qualitative point of view, however, two features of this spatio-temporal development, $I_{comp}(x)$, are remarkable: (*a*) The amplitude of the compound current decreases with increasing time. (*b*) There is a significant spatial dispersion of $I_{comp}(x)$ with increasing time. This phenomenon applies in particular to the compound repolarization current, whereas, during the first 10 ms, the leading depolarization wave remains relatively sharp.

The explanation of this behavior is quite simple. The depolarization current of fibers with lower propagation velocity is compensated by the repolarization current of the faster fibers. This leads to a general decrease of the compound current intensity. Only the depolarization current of the fastest fibers is not compensated by antiparallel currents, so that a sharply peaked wave remains at the propagation front. The asymmetry of the single fiber action current, $I_x(t)$, is the reason why the analogous phenomenon at the slow end of the distribution is only weakly pronounced.

Now we are in the position to give a realistic picture of the current configuration investigated in this study. The depolarization front reaches the scanning line 6 ms after the stimulation. At this instant, the nerve tissue below the magnetometer coil carries a current peak of 50 mm half height width in the x-direction. The geometrical parameters of the experimental setup, namely the coil diameter and the coil to source distance, are of the same order of magnitude as the extent of the source. Under these conditions, the model of the equivalent current dipole still provides a good approximation of the magnetic field generated by the real source (25). The current dipole intensity equivalent to the real current distribution is reduced by a factor of seven with respect to a synchroneous activity of the fibers at $t = 0$.

3 ms later, the negative part of $I_{comp}(x)$ reaches the scanning line. With 250 mm, the spatial extent of this current distribution exceeds the size of the critical parameters of the experimental setup, and the corresponding magnetic field does not fit the field of a dipolar source. In addition, the current amplitude is five times weaker than in the case of the depolarization front and vanishes in the noise. For these reasons, the compound repolarization current encountered in this situation is not a source appropriate for a biomagnetic localization. At some earlier instant, say, 2 ms after the stimulation, the situation is different: both de- and repolarization currents are spatially limited to a few centimeters and might allow a successful localization of the source. In this case, the second term of the current multipole expansion should be taken into account to provide an adequate description of the entire source, consisting of both antiparallel parts of the real current distribution (13). The recording of these early fields at positions close to the stimulator is not easy due to the overload of the receiver after the stimulation pulse. Recently, a biphasic MCAF of the ulnar nerve was indeed detected at the elbow (26).

5. CONCLUSION

In this report we have presented a functional localization of bioelectrically active tissue. The biomagnetic field recorded from a linear scan was used to determine the two-dimensional position of the source in the cross-section of the upper arm. The basis of this procedure was the model of a pointlike current dipole. Taking advantage of the simple anatomic structure of the active tissue, a second independent localization was obtained by a CT-image of the upper arm cross-section. The two results agree with a deviation of <2 mm, the best confirmation of a biomagnetic localization in vivo reported to date. This is a promising issue. It will be an important task to find out which situations can produce results of similar precision. In particular, a systematic and comprehensive study of the impact of volume currents on the validity of biomagnetic localizations will be of great relevance. A second question concerns the validity of localizations of more complicated sources, such as currents of larger spatial extent or complex current structures.

Although the weakness of MCAFs makes their recording somewhat difficult, we want to suggest that more such studies be performed. These current sources combine the benefits of well-defined anatomic and electric structures. The first advantage permits an easy validation by standard imaging techniques. The second advantage should be seen in the light of the poor knowledge about most bioelectric sources. Only a few model calculations of biologic currents have been reported to date (27). In this study, the calculation of the real current distribution in the nerve justifies the use of the equivalent current dipole model. The conditions of this experiment were chosen such that a source with a most simple structure was to be analyzed. On the other hand, it is interesting to note that even in this case there is a fine structure of the source which is not reflected in the biomagnetic field outside. Some 5,000 single fiber currents sum up in the nerve bundle in a way that most of their magnetic action in the surrounding is compensated.

Further studies on MCAFs could deal with more complex but still well-defined current sources. We have shown that under different circumstances, peripheral nerves carry biphasic currents that can be modeled by quadrupolar sources. In addition, the stimulation of particular anatomic nerve configurations such as bifurcations, or the synchronized stimulation of two or more nerves, will generate current distributions with a variety of structures. We believe that such investigations could contribute relevant experimental background when the biomagnetic method becomes established as a clinical tool.

The recording of the contrast enhanced CT-image by Dr. Berger of the Radiology Department of the Berlin Steglitz Clinic is gratefully acknowledged. We also thank Dr. Maria Peters and Dr. Riitta Hari for sending us their manuscripts before publication.

Received for publication 30 September 1988 and in final form 30 December 1988.

REFERENCES

1. Ricci, G. B., R. Leoni, G. L. Romani, F. Campitelli, S. Buonomo, and I. Modena. 1985. 3-D Neuromagnetic localization of sources of interictal activity in cases of focal epilepsy. *In* Biomagnetism: Applications and Theory. H. Weinberg, G. Stroink, and T. Katila, editors. Pergamon Press, New York. 304–310.
2. Sutherling, W. W., P. H. Crandall, J. Engel, T. M. Darcey, L. D. Cahan, and D. S. Barth. 1987. The magnetic field of complex partial seizures agrees with intracranial localization. *Ann. Neurol.* 21:548–558.
3. Sutherling, W. W., P. H. Crandall, L. D. Cahan, and D. S. Barth. 1988. The magnetic field of epileptic spikes agrees with intracranial localizations in complex partial epilepsy. *Neurology.* 38:778–786.
4. Wikswo, J. P., J. P. Barach, and J. A. Freeman. 1980. The magnetic field of a nerve impulse: first measurements. *Science (Wash. DC).* 208:53–55.
5. Wikswo, J. P., G. S. Abraham, and V. R. Hentz. 1985. Magnetic assessment of regeneration across a nerve graft. *In* Biomagnetism: Applications and Theory. H. Weinberg, G. Stroink, and T. Katila, editors. Pergamon Press, New York. 88–92.
6. Mizutani, Y., and S. Kuriki. 1986. Somatically evoked magnetic fields in the vicinity of the neck. *IEEE (Inst. Electr. Electron. Eng.) Trans. Biomed. Eng.* BME-33:510–516.
7. Erné, S. N., G. Curio, L. Trahms, Z. Trontelj, and P. Aust. 1988. Magnetic activity of a single peripheral nerve in man. *In* Biomagnetism '87. K. Atsumi, M. Kotani, S. Ueno, T. Katila, and S. J. Williamson, editors. Tokyo Denki University Press, Tokyo. 166–169.
8. Erné, S. N., H. D. Hahlbohm, H. Scheer, and Z. Trontelj. 1981. The Berlin magnetically shielded room (BMSR). Section B. Performances. *In* Biomagnetism. S. N. Erné, H. D. Hahlbohm, and H. Lübbig, editors. DeGruyter, Berlin. 79–87.
9. Erné, S. N., H. D. Hahlbohm, and J. Palow. 1981. The Berlin magnetically shielded room (BMSR). Section C. Periphery. *In* Biomagnetism. S. N. Erné, H. D. Hahlbohm, and H. Lübbig, editors. DeGruyter, Berlin. 89–92.
10. Zimmerman, J. E., P. Thiene, and J. T. Harding. 1970. Design and operation of stable rf-biased superconducting point-contact quantum devices, and a note on the properties of perfectly clean metal contacts. *J. Appl. Phys.* 41:1572–1580.
11. Scheer, H. J. 1987. Line frequency rejection for biomedical application. *IEEE (Inst. Electr. Electron. Eng.) Trans. Biomed. Eng.* BME-34:68–69.
12. Jackson, J. D. 1962. Classical Electrodynamics. John Wiley & Sons, New York. 141–145.
13. Erné, S. N., L. Trahms, and Z. Trontelj. 1988. Current multipoles as sources of biomagnetic and bioelectric fields. *In* Biomagnetism '87. K. Atsumi, M. Kotani, S. Ueno, T. Katila, and S. J. Williamson, editors. Tokyo Denki University Press, Tokyo. 302–305.
14. Williamson, S. J., and L. Kaufman. 1981. Magnetic fields of the cerebral cortex. *In* Biomagnetism. S. N. Erné, H. D. Hahlbohm, and H. Lübbig, editors. DeGruyter, Berlin. 353–402.
15. Cohen, D., and H. Hosaka. 1976. Magnetic field by a current dipole. *J. Electrocardiol.* 9:409–417.
16. Katila, T., 1981. Instrumentation for medical applications. *In* Biomagnetism. S. N. Erné, H. D. Hahlbohm, and H. Lübbig, editors, DeGruyter, Berlin. 3–31.
17. Peters, M. J., and P. Elias. 1988. On the magnetic field and the electrical potential generated by bioelectric sources in an anisotropic volume conductor. *Med. Biol. Eng. Comp.* 26:617–623.
18. Geddes, L. A., and L. E. Baker. 1967. The specific resistance of biological material, a compendium of data for the biomedical engineer and physiologist. *Med. Biol. Eng.* 5:271–293.
19. Stanley, P. C., T. C. Pilkinton, and M. N. Morrow. 1986. The effects of thoracic inhomogeneities on the relationship between epicardial and torso potentials. *IEEE (Inst. Electr. Electron. Eng.) Trans. Biomed. Eng.* BME-33:273–284.
20. Huxley, A. F. 1959. Can a nerve propagate a subthreshold disturbance? *J. Physiol. (Lond.)* 148:80P–81P.
21. Scott, A. C. 1975. The electrophysics of a nerve fibre. *Rev. Mod. Phys.* 47:487–533.

22. Stegeman, D. F., and J. P. C. deWeerd. 1982. Modeling compound action potentials of peripheral nerves in situ. I. Model description: evidence of a nonlinear relation between fibre diameter and velocity. *Electroencephalogr. Clin. Neurophysiol.* 54:436–448.

23. Cummins, K. L., L. J. Dorfman, and D. H. Perkel. 1979. Nerve fiber conduction-velocity distributions. II. Estimation based on two compound action potentials. *Electroencephalogr. Clin. Neurophysiol.* 46:647–658.

24. Stegeman, D. F., and J. P. C. deWeerd. 1982. Modeling compound action potentials of peripheral nerves in situ. II. A study of the influence of temperature. *Electroencephalogr. Clin. Neurophysiol.* 54:516–529.

25. Okada, Y. 1985. Discrimination of localized and distributed dipole sources and localized single and multiple sources. *In* Biomagnetism: Applications of Theory. H. Weinberg, G. Stroink, and T. Katila, editors. Pergamon Press, New York. 266–272.

26. Hari, R., J. Hällström, J. Tiihonen, and S.-J. Joutsiniemi. 1989. Multi-channel detection of magnetic compound action fields of median and ulnar nerves. *Electroencephalogr. Clin. Neurophysiol.* 72:277–280.

27. Uchikawa, Y., and S. N. Erné. 1988. Modelling of the Wolff-Parkinson-White syndrome with magnetocardiography. *In* Biomagnetism '87. K. Atsumi, M. Kotani, S. Ueno, T. Katila, and S. J. Williamson, editors. Tokyo Denki University Press, Tokyo. 322–325.